Protein Science (1996), 5:434–441. Cambridge University Press. Printed in the USA.

The structure of bovine mitochondrial adenylate kinase: Comparison with isoenzymes in other compartments

G.J. SCHLAUDERER AND G.E. SCHULZ

Institut für Organische Chemie und Biochemie, Albertstr. 21, D-79104 Freiburg im Breisgau, Germany

(RECEIVED October 9, 1995; ACCEPTED December 11, 1995)

Abstract

In vertebrates, there are different adenylate kinases in the compartments cytosol, mitochondrial intermembrane space, and mitochondrial matrix. Here, we report the spatial structure of the intermembrane species established in two crystal forms by X-ray diffraction analyses at 1.92 and 2.1 Å resolution. In both structures, the enzyme is unligated, and thus in an "open" conformation. The enzyme was prepared from bovine liver, containing at least five variants arisen from posttranscriptional and posttranslational modifications. It could only be crystallized after removing some of these variants. A comparison with the known structures of the adenylate kinases from cytosol and mitochondrial matrix reveals structural differences that should play a role in protein targeting because none of these enzymes contains a cleavable signal peptide. A further comparison with adenylate kinases from Gram-positive bacteria showed that the structural Zn^{2+} ion of these species is replaced by a strictly conserved assembly of hydrogen bonded residues.

Keywords: adenylate kinase; mitochondrial intermembrane space; posttranslational modifications; protein targeting; X-ray diffraction

Adenylate kinases catalyze the reaction $Mg^{2+}ATP + AMP \rightleftharpoons Mg^{2+}ADP + ADP$. They are ubiquitous and most abundant in cells with a high energy turnover (Noda, 1973). Besides about 35 published amino acid sequences, high-resolution crystal structures are known for the enzymes from pig muscle cytosol (AK1, Dreusicke et al., 1988), from bovine mitochondrial matrix (AK3, Diederichs & Schulz, 1991), from *Escherichia coli* (Müller & Schulz, 1992; Berry et al., 1994), and from yeast (Abele & Schulz, 1995). The enzymes belong to the larger family of nucleoside monophosphate kinases, among which the UMP(CMP-)-kinases are closely (Müller-Dieckmann & Schulz, 1995) and the GMP-(Stehle & Schulz, 1992) and TMP-kinases (Wild et al., 1995) only distantly related. A comparison of the structures with and without substrates revealed large domain movements during catalysis (Schulz et al., 1990; Vonrhein et al., 1995).

Reprint requests to: Georg E. Schulz, Institut für Organische Chemie und Biochemie, Albertstr. 21, D-79104 Freiburg im Breisgau, Germany; e-mail: schulz@chemie.uni-freiburg.de.

Abbreviations: AK1, adenylate kinase from cytosol; AK2, adenylate kinase from mitochondrial intermembrane space; AK3, adenylate kinase from mitochondrial matrix; *B*-factor, crystallographic temperature factor; CORE, domain defined as the bulk of the adenylate kinase polypeptide; LID, domain closing over bound ATP; NMP_{bind}, domain closing over bound NMP, e.g., AMP.

The adenylate kinases of vertebrates are compartment-specific; AK1 is in the cytosol, AK2 in the intermembrane space of mitochondria (Markland & Wadkins, 1966; Font & Gautheron, 1980), and AK3 in the mitochondrial matrix. The three isoenzymes are important for the homeostasis of the adenine nucleotide metabolism. They are produced in the cytosol; the expression is tissue-specific and developmentally regulated (Tanabe et al., 1993). The signals targeting AK2 and AK3 to the mitochondrial compartments are still unknown (Magdolen et al., 1992), the sequences contain no conventional signal peptides. The isoenzymes are homologous with around 30% identical amino acids. The reported structure of AK2 now permits a structural comparison between all three species.

Results and discussion

Enzyme isolation and crystallization

AK2 has been isolated from the intermembrane space of bovine liver mitochondria according to Tomasselli and Noda (1980). Because AK2 undergoes posttranscriptional and posttranslational modifications at the N- and C-termini, the enzyme preparations were heterogeneous and thus hard to crystallize. An overview of the modifications is given in Figure 1. Kishi et al. (1987) and

```
            1   3              233              240
            |   |               |                |
AK2-A     M-A-P-N-V-P ... A-T-C-K-D-L-V-M-F-I
AK2-A1      A-P-N-V-P ... A-T-C-K-D-L-V-M
AK2-A1a     A-P-N-V-P ... A-T-C-K-D-L-V-M-F-I
AK2-A2        D-V-P ... A-T-C-K-D-L-V-M
AK2-B     M-A-P-N-V-P ... A-T-S
AK2-B1      A-P-N-V-P ... A-T-S
AK2-B2        D-V-P ... A-T-S
```

Fig. 1. Posttranscriptional (AK2-A and AK2-B) and posttranslational (indices 1, 1a, 2) modifications of bovine adenylate kinase from the mitochondrial intermembrane space. AK2-A and AK2-B refer to the sequences translated from mRNA.

Tanaka et al. (1990) found that AK2-A and AK2-B are produced during mRNA splicing and that AK2-A is dominant (5:1) in heart, whereas AK2-B is the major (5:1) species in liver. Actually isolated from heart and sequenced was the enzyme AK2-A_1 (Frank et al., 1986), lacking the N-terminal Met- and the C-terminal -Phe-Ile of the translated mRNA sequence. A later carboxypeptidase digest of the same enzyme preparation revealed about 30% Ile and Phe besides the prevalent Met, Val, and Leu, and indicated, together with the then known gene sequence, that there exists yet another minor variant, AK2-A_{1a}, with a complete C-terminus. AK2-A_2 arises from a posttranslational modification cutting two residues and deamidating Asn 3.

The enzyme AK2-B has a shortened C-terminus with Ser instead of Cys as the last residue. It is further modified at the N-terminus to yield AK2-B_1 and AK2-B_2. In liver, the ratio between AK2-B_1 and AK2-B_2 is 4:1 (Schneemann, 1986); and the same ratio is found for AK2-A_1 and AK2-A_2 in heart (Jäger, 1985). Most conspicuously, the specific activities of the minor variants AK2-A_2 and AK2-B_2 of 1,600 U/mg are twice as high as the activities of the major variants AK2-A_1 and AK2-B_1. This difference finds no structural explanation because the N-terminus is mobile (see below).

Because we isolated the enzyme from liver, our major species was AK2-B and its derivatives (Kishi et al., 1987). We dispensed with the minor species AK2-B_2 (and AK2-A_2) by chromatofocusing, making use of the isoelectric point differences between pI 8.4 for AK2-B_1 (and -A_1) and pI 7.6 for AK2-B_2 (and -A_2). The remaining enzyme preparation is likely to consist of AK2-B_1 and AK2-A_1 at a ratio of 5:1. After crystallization, we found a well-defined C-terminal Ser in the structure, which also participates in a packing contact in both crystal forms (see below). Therefore, the crystals contain AK2-B_1, and cocrystallization with the minor variant AK2-A_1 seems unlikely.

The first crystals were grown at pH 7.8 using ammonium sulfate as a precipitant. They belonged to space group $P2_12_12_1$ with cell parameters 44.2 × 50.1 × 123.3 Å^3, contained one molecule per asymmetric unit, and were named "form-S." Later, a second crystal, "form-P," was grown from PEG that was isomorphous to form-S, except for a *c*-axis that was 1.0 Å shorter.

Structure determination and model quality

The structure was solved in crystal form-P by multiple isomorphous replacement and solvent flattening at 3 Å resolution (see below). The resulting electron density map was not clear enough to place the polypeptide chain, but it sufficed to recognize the chain fold of the CORE and NMP_{bind} domains known from homologous enzymes. The positioned CORE domain was a satisfactory starting point for a simulated annealing refinement at 2.5 Å resolution, which yielded most of the model after four rounds. Subsequently, water was introduced and the resolution extended to 1.92 Å. The form-S structure was established by refining the form-P model against the form-S data set in the slightly expanded unit cell and by refitting the water molecules.

The structure analyses data are given in Table 1. The models of the two crystal forms resemble each other closely, except for the *B*-factor of the sulfate bound at the position of the ATP-β-phosphate in the giant anion hole (Dreusicke & Schulz, 1986). In form-P, with the lower sulfate concentration, the sulfate *B*-factors are much higher, presumably compensating for a lower occupancy. The coordinate error estimates are around 0.3 Å, in agreement with the RMS ΔC^α deviation between the two models (see Fig. 2A). Program PROCHECK (Laskowski et al., 1993) showed all (non-Gly and non-Pro) residues of both models in allowed regions. A comparison of the backbone dihedral angles resulted in low averages of $\langle|\Delta\phi|\rangle = 5°$ and $\langle|\Delta\psi|\rangle = 5°$, indicating good model quality.

The ΔC^α distribution in Figure 2A shows deviations at the mobile N-termini and in domains NMP_{bind} and LID that move during catalysis and are sensitive to small environmental changes. The LID motion between forms-P and -S corresponds

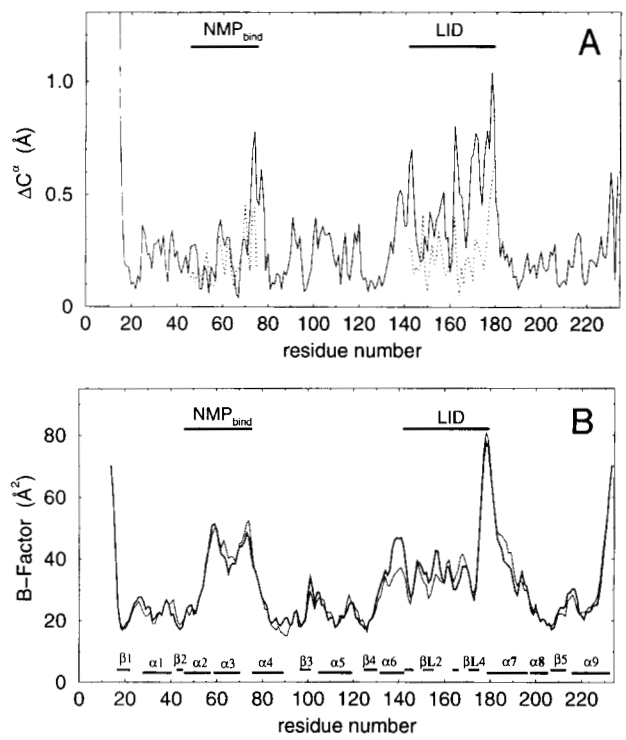

Fig. 2. Structural comparison of AK2-B_1 in crystal forms-P and -S. **A:** Residual ΔC^α distribution after the best superposition, the mobile domains NMP_{bind} and LID are indicated and also superimposed separately (dotted lines). **B:** B-factor distribution for crystal form-P (thick line) and -S (thin line). The secondary structures as well as domains NMP_{bind} and LID are given. Because they are absent in the small variants of this enzyme family, the four β-strands of the LID domain carry separate names: β_{L1}, β_{L2}, β_{L3}, and β_{L4}.

Table 1. *Refined models of mitochondrial AK2-B_1*

	Form-P[a]	Form-S[a]
Space group	$P2_12_12_1$	$P2_12_12_1$
Cell parameters (Å^3)	44.2 × 50.1 × 122.3	44.2 × 50.1 × 123.3
Resolution (Å)	10–1.92	10–2.1
Completeness (%)	98	92
Unique reflections in range	20,850	15,064
R_{sym} (%)	7.7	5.0
Non-hydrogen protein atoms[b]	1,699	1,699
Water molecules plus sulfate	118	101
R-factor (%)	22.2	22.2
RMS deviations of		
Bond lengths (Å)	0.011	0.010
Bond angles (°)	1.6	1.6
Luzzati (1952) error estimate (Å)	0.27	0.29
Read (1986) σ_A-error estimate (Å)	0.28	0.32
Average B-factors of [c]		
All protein atoms[b] (Å^2)	33	33
Water molecules (Å^2)	50	50
Sulfate ion (Å^2)	58	39

[a] P, polyethyleneglycol; S, ammonium sulfate.
[b] Residues 14–233.
[c] RMS B-factor difference between neighboring main-chain atoms was 1.3 (3.6) Å^2 and between atoms connected via a third atom 2.4 (5.3) Å^2, the side-chain values being in parentheses.

to a smallish 4° rotation, probably caused by the sulfate occupancy difference. The B-factor distributions in Figure 2B give a similar impression: high mobilities at the termini and at domains NMP_{bind} and LID. Conspicuous is the soft spot around position 178 at the "trigger" of the LID motion (Müller-Dieckmann & Schulz, 1995) and the B-factor difference around position 140, where the well-occupied sulfate of form-S causes the fixation of Arg 143 in its environment.

Crystal contacts

On substrate binding, the adenylate kinase conformations change dramatically from an "open" to a compact shape (Schulz et al., 1990). Without bound substrates, the reported AK2 structures are in their "open" conformations, which are more susceptible to external influences than the compact ones. Therefore, we analyzed the packing contacts and listed them for both crystal forms in Table 2. The largest contacts, I-II and I-III, form the 2_1-screw along the a-axis, which corresponds well with the crystal habit showing columns with a 10:1 elongation along this axis. Altogether, the molecules in crystal forms-P (-S) bury 29% (30%) of their solvent-accessible surface on crystallization, pointing to an appreciable packing influence. Because the mobile domains NMP_{bind} and LID participate in contacts I-II and I-VI, their positions relative to CORE are likely to be affected by the packing. It should be noted that the C-terminal residue 233 is involved in contact I-VI, which renders the presence of the C-terminally prolonged AK2-A_1 unlikely.

Structure of AK2-B_1

The chain fold of the crystalline enzyme is depicted in Figure 3 and Kinemage 1. Like the other NMP-kinases, it contains a central parallel five-stranded β-sheet surrounded by α-helices. Both molecules contain a sulfate at the β-phosphate position of ATP. The adenylate kinase structures have been subdivided into three domains (Schulz et al., 1990): NMP_{bind} (here residues 46–75) closing over bound AMP, LID (here 142–179) closing over bound ATP, and the remaining CORE domain (see below Fig. 7). The 13 N-terminal residues have no defined conformation. The C-terminus has good density for Ser 233, including its carboxylate. It remains a puzzle, however, why the N-terminal modi-

Table 2. *Packing contacts for crystal form-P of AK2-B_1*

Contacting molecules[a]	Contacting segment[b]	Contact area[c] (Å^2)	Number of hydrogen bonds[c]
I-II	a–b	927 (975)	11 (10)
I-III	b–a	927 (975)	11 (10)
I-IV	c–d	461 (441)	5 (5)
I-V	d–c	461 (441)	5 (5)
I-VI	e–f	272 (277)	1 (1)
I-VII	f–e	272 (277)	1 (1)

[a] Reference molecule is I (x, y, z). Symmetrically related molecules are II ($x + 1/2$, $1/2 - y$, $-z$), III ($x - 1/2$, $1/2 - y$, $-z$), IV ($-x$, $y + 1/2$, $1/2 - z$), V ($-x$, $y - 1/2$, $1/2 - z$), VI ($x + 1$, y, z), and VII ($x - 1$, y, z).
[b] Residues in the contacts that contain at least one atom with a distance below 4.5 Å to a neighbor are: a = 35, 38–39, 151, 155, 159–164, 167–170, 175, 218–219, 221–222, 225; b = 47–48, 51–52, 69–71, 104, 145, 147–148, 174–180, 183, 187; c = 110, 113–114, 117, 200–201, 204–206; d = 14, 88–92, 94, 119–121; e = 15–16, 39–40, 154, 225, 229, 233; f = 70–74.
[c] Contact area is half the buried area (X-PLOR, probe radius 1.4 Å). Values in parentheses are for crystal form-S.

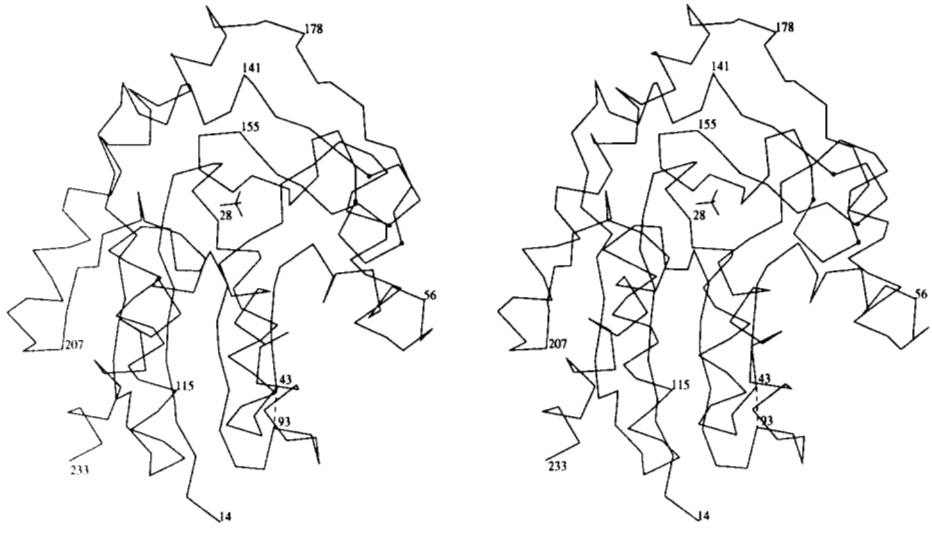

Fig. 3. C^{α} backbone fold of AK2-B_1 in crystal form-P. Note that 13 residues are missing at the N-terminus. The sulfate at the β-phosphate position of ATP and the disulfide bridge 43–93 are depicted. Some residues are labeled. The four residue positions where the structural Zn^{2+} is bound in the homologous Gram-positive bacteria (Fig. 4) are marked by dots.

fication producing AK2-B_2 from AK2-B_1 (Fig. 1) gives rise to an enzyme with doubled catalytic rate, although it does not change the structured part of the enzyme.

Domains NMP_{bind} and LID are not arrested by bound substrates and are therefore free to assume various positions relative to CORE. A comparison with unligated AK1 indicates a 17° rotation of NMP_{bind} to a more open conformation in AK2 (Table 3). When compared with AK3, the LID domain of AK2 shows a 73° rotation to a more closed conformation. A comparison with the homologous yeast enzyme in its compact form (Abele & Schulz, 1995), however, indicates that there remains still a 36° rotation to the "closed" state. These large differences between "open" conformations are a consequence of crystal packings; the positions of NMP_{bind} and LID are only well-defined in their "closed" states assumed on substrate binding.

Domain NMP_{bind} consists essentially of two α-helices. In contrast the LID domain contains four antiparallel β-strands with a more elaborate construction. It is remarkable that the LID domain of adenylate kinases from Gram-positive bacteria harbor a structural Zn^{2+} (Gilles et al., 1994), which is held by four side chains, most of which are cysteines. In the LID domains of eucaryotes and some procaryotes, this Zn^{2+} is replaced by a hydrogen bonding web, as depicted in Figure 4 and Kinemage 2, which is strictly conserved. This web seems to substitute the bound Zn^{2+} ion efficiently.

Because the 38-residue LID domain moves like a solid block on ATP binding (Schulz et al., 1990), it could be an independent domain grafted from other proteins. A search through the Protein Data Bank using program DALI (L. Holm, pers. comm.), however, yielded only rubredoxin as a distant relative. Rubredoxin binds its Fe^{3+} ion similarly between two β-turns (Watenpaugh et al., 1980) as some adenylate kinases bind their structural Zn^{2+} ion (Fig. 4).

Using the program GRASP, we inspected the electrostatic potentials of adenylate kinases. Figure 5 shows that the large cleft accommodating the phosphates of ATP and AMP has a rather positive potential. It is compensated by negative potentials at the right-hand side of Figure 5 (at the left-hand side of Fig. 3) between strand β4 (label 130) and helix α7, as well as between helices α5 (label 114) and α8. In contrast to the positive cleft potential that attracts the substrates, the negative patches find no explanation. It is conceivable, though, that the patch at β4 and α7 affects the LID domain motion (see below).

Table 3. *Superpositions of the bovine isoenzymes AK1, AK2 (form-P), and AK3 (molecule-I)*[a]

	AK2 RMS ΔC^{α} (Å)			AK3 RMS ΔC^{α} (Å)		
	NMP_{bind}	LID	CORE	NMP_{bind}	LID	CORE
AK1	0.5 (17°)	–	1.7 (0.9;98)	1.0 (21°)	–	1.8 (0.9;90)
AK2	–	–	–	1.1 (36°)	1.4 (73°)	2.0 (0.8;88)

[a] Domains are defined in Figure 7. Alternative form-S of AK2 and molecule-II of AK3 resemble their counterparts closely and need not be compared separately. Polar rotation angles given in parentheses for domains NMP_{bind} and LID refer to a prior superposition of CORE. For CORE, values in parentheses are the RMS ΔC^{α} and the remaining number of residues for a 1.5 Å cut-off superposition.

Comparison with the other isoenzymes

The three bovine isoenzymes AK1, AK2, and AK3 are depicted in Figure 6 and their sequences are aligned in Figure 7. At around 30% identical amino acids, the isoenzymes are homologous in sequence and chain fold. All crystallized species contain a sulfate at the β-phosphate position of ATP, and AK3 contains AMP in addition. The most obvious difference is the lacking LID domain in cytosolic AK1. Without LID, the ATP-specificity of AK1 is reduced, permitting further functions as, for instance, the production of thiamin *tri*phosphate and AMP from the usual *-di*phosphate and ADP (Miyoshi et al., 1990).

Without ATP present, the LID domains are in their less well-defined "open" conformations. Accordingly, the LID positions of AK2 and AK3 differ grossly (Fig. 6). Still, the internal structures of the LID domains agree well with an RMS ΔC^{α} of only 1.4 Å (Table 3). The LID sequence is very well conserved dur-

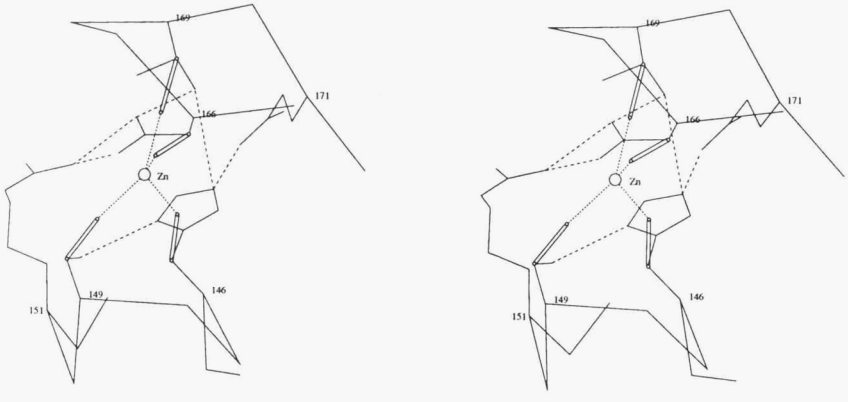

Fig. 4. C^{α} backbone (144–153, 165–172) and side chains (His 146, Ser 149, Arg 151, Asp 166, Thr 169, Glu 171) forming the hydrogen bonding web in LID domains that corresponds to the structural Zn^{2+} ion found in adenylate kinases of Gram-positive bacteria. Web residues are strictly conserved. A model of the four cysteine side chains of Gram-positive bacteria is superimposed. The sulfur positions are geometrically optimized to bind the putative Zn^{2+} ion. C^{β}-S^{γ} bonds and Zn^{2+} are emphasized by light double lines and light balls. In a superposition with rubredoxin (Watenpaugh et al., 1980), the four cysteine residues and the Fe^{3+} ion of rubredoxin are at positions equivalent to the modeled Cys and Zn^{2+} positions of Gram-positive bacteria. Moreover, the depicted part of the main chains of AK2 and rubredoxin superimposes with an RMS ΔC^{α} of 1.3 Å, indicating an evolutionary convergence to a common metal-binding site.

ing evolution; for instance, there are 63% identical amino acids between AK2 and AK3 (Fig. 7). Because LID is not required for catalysis (absent in AK1) and still much better conserved than the rest of the molecule, we suggest that it interacts with other cellular components fulfilling further functions (Goelz & Cronan, 1982).

Superpositions of the CORE domains yield RMS ΔC^{α} values of about 2.0 Å, but the central parts (around 90 residues) deviate by only 0.9 Å (Table 3). A closer inspection shows that the largest differences are in the chain connections to the NMP_{bind} and LID domains, which are affected by the domain motions, i.e., here in the absence of substrates by crystal packing (Gerstein et al., 1993).

The greatest differences between the three isoenzymes occur at the amino terminal end of the central parallel β-sheet, where the N- and C-termini, as well as the loops around residues 93 and 117 containing insertions/deletions (Fig. 7), meet each other. Moreover, AK2 has 16 and AK3 6 residues before the start of the first β-strand where the consensus structure begins (Fig. 7). In both cases, most of the N-terminal extension residues have no structure. In contrast, AK1 has eight residues before the start forming a stable α-helix. At the C-terminus, the consensus structure ends at residue 229. Here, AK2 and AK1 have 4- and 3-residue extensions, adding another helix turn. In contrast, AK3 has a 14-residue C-terminal extension that adds another helix turn and is structureless for the last 10 residues.

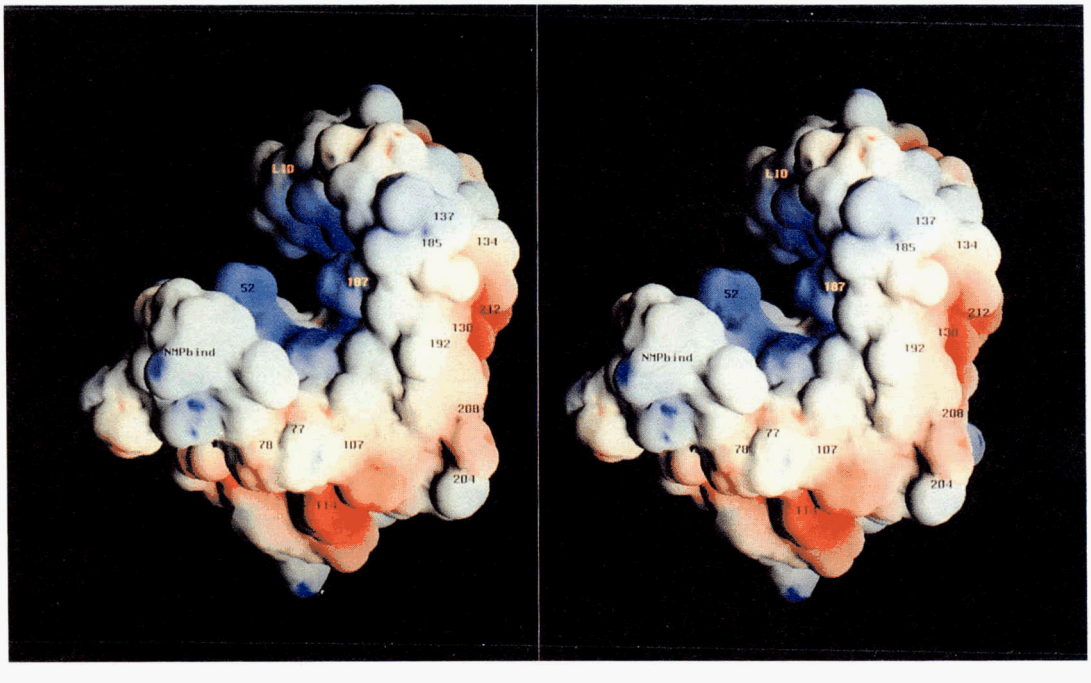

Fig. 5. Electrostatic potential on the surface of AK2 as calculated with the program GRASP (Nicholls et al., 1991). Blue and red mark positive and negative potentials, respectively. The potentials range between −11.4 and +15.9, the colors run from −7.7 to +10.8 (all in kT-units). The two mobile domains and several residue positions are labeled.

Fig. 6. Ribbon plots of the three bovine isoenzymes AK1 (cytosol), AK2 (mitochondrial intermembrane space), and AK3 (mitochondrial matrix). β-Strands are green, ligated sulfates and AMP are blue, and disulfide of AK2 is purple. For AK1, we used the chain fold of the pig enzyme, which is most likely identical to the bovine species because there are only nine amino acid exchanges (Fig. 7).

Because none of the adenylate kinase genes contains a signal sequence (Yamada et al., 1989; Tanaka et al. 1990), the targeting (Douglas et al., 1986; Glick & Schatz, 1991) to the respective mitochondrial compartments has remained unexplained. Now, the three-dimensional structures show that cytosolic AK1 has a defined structure for its complete chain, whereas the others contain mobile extensions: AK2 has a structureless 13-residue N-terminal extension containing four prolines and two negative charges. Because of the negative charges, this extension cannot be a conventional (but noncleaved) signal peptide (Douglas et al., 1986). AK3 has a structureless 5-residue N-terminal extension with one positive charge and a 10-residue C-terminal extension that begins after a proline and has zero net charge. Given this difference between AK1 and the others, it is tempting to speculate that the mobile extensions play a role in targeting to mitochondria.

A comparison between the electrostatic potentials on the protein surfaces shows no significant differences between AK1, AK2, and AK3, and thus does not allow a conclusion concerning protein targeting (Fig. 5). It shows further that these species resemble each other with respect to the prominent patches. In particular, the negative patch between strand β4 (label 130) and helix α7 appears to be a general property of this enzyme family. This negative potential seems to be important for catalysis because the yeast enzyme mutation Asn 169 → Asp at this patch (equivalent position in AK2 is 180, Figs. 5, 7) reduced the catalytic rate by a factor of 7 (Spuergin et al., 1995). Apparently, the additional negative charge perturbs the electrostatic balance in the enzyme. This is corroborated by a comparison with the other known sequences showing that position 180 always accommodates neutral or positively charged residues, as, for instance, an arginine in AK3.

Materials and methods

Protein purification and crystallization

AK2 was prepared from bovine liver mitochondria. After about 1 week, we obtained around 10 mg AK2 from 6 kg liver. The enzyme was stored at −20 °C in storage buffer for up to 2 weeks. The last step of the purification was a chromatofocusing column that separated the major component AK2-B_1 (probably together with some AK2-A_1) with pI 8.4 from the minor component AK2-B_2 with pI 7.6. The pI 8.4 of the major component was also found with a recombinant AK2-B produced (Greschik, 1994) from a clone gratefully received from A. Nakazawa (Ube, Japan).

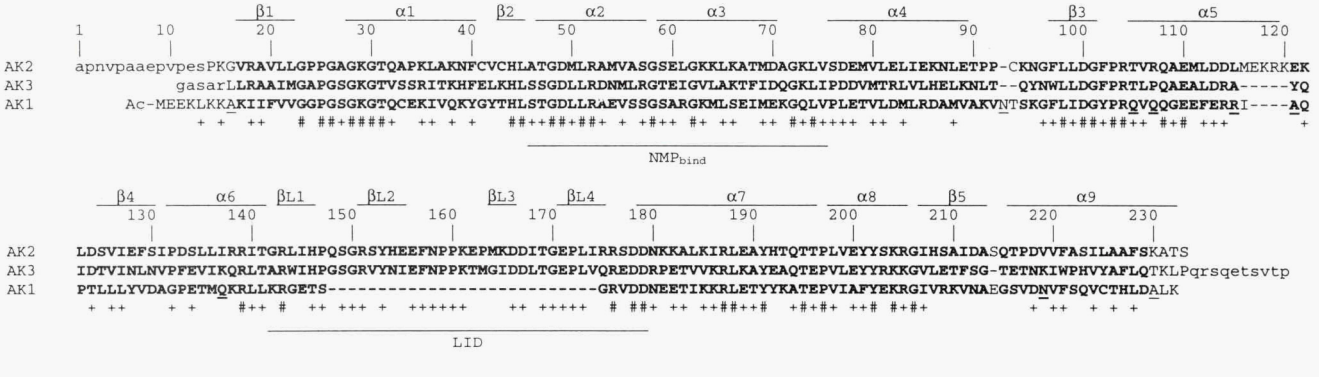

Fig. 7. Structural sequence alignment of the three bovine isoenzymes AK2-B_1 (Frank et al., 1986; Kishi et al., 1987), AK3 (Tomasselli et al., 1986), and AK1 (Kuby et al., 1984) with the numbering of AK2. It is assumed that bovine AK1 has the same chain fold as the pig enzyme (Heil et al., 1974), the nine exchanged residues are underlined. Sequence identities are marked (+ for two sequences, # for three). The secondary structures of AK2 are introduced. The β-strands of the LID domain carry separate names: β_{L1}, β_{L2}, β_{L3}, and β_{L4}, because they are absent in the small variants of the enzyme family. A consensus structure had been derived from a structural alignment of six sequences by Vonrhein et al. (1995); it is marked by bold print. The CORE domain complements domains NMP_{bind} and LID and contains 138 residues in the consensus region. All other residues are depicted as normal upper and lower case letters, where the lower case denotes residues that are mobile and therefore not visible in the crystal structure. At the C-terminus of AK3, three residues that are clearly held by a crystal contact and not by the bulk protein are given in lower case.

Table 4. *Phase determination of AK2-B_1 crystal form-P*

Crystal soaking			Data collection			Heavy atom parameters		
Compound[a]	Concentration (mM)	Time (d)	Resolution (Å)	Completeness (%)	R_{sym} (%)	R_{iso}[b] (%)	Sites[c]	Phasing power[d] in ∞–4.8 Å
MMA	5	3	3.0	87	4.7	34	.24/.12/.18 .10/.69/.14 .89/.67/.08	2.3
Terpy	Saturated	10	3.0	85	4.5	25	.81/.09/.05 .88/.73/.07	1.4
PHMB	1	12	3.4	81	4.8	26	.24/.12/.18 .21/.14/.16	2.1
$K_2Pt(SCN)_4$	0.5	1	4.8	83	6.9	26	.53/.22/.13	1.2

[a] Methylmercury acetate, ter(pyridinium)platinum-II chloride, *p*-(hydroxymercury)-benzoate.
[b] $R_{iso} = 2 \cdot \Sigma|F_{der} - F_{nat}|/\Sigma(F_{der} + F_{nat})$ is the difference between derivative and native data.
[c] All sites are approximately equally occupied, the first site of MMA and both sites of the PHMB derivative are at the only free thiol of Cys 41.
[d] The phasing power is the average heavy atom structure factor divided by the average error. Derivatives MMA, Terpy, and PHMB have phasing powers of 1.0, 0.6, and 0.9, respectively, in their full resolution ranges.

Using the hanging drop method, the purified protein was crystallized in a drop starting with about 15 mg/mL protein, 50 mM Tris-HCl, pH 7.8, 1.4 M ammonium sulfate, 5 mM $MgSO_4$, 4% PEG-1000, 5 mM β-mercaptoethanol, and 1 mM EDTA. The reservoir contained 2.05 M ammonium sulfate, 50 mM Tris-HCl, pH 7.8, 5 mM β-mercaptoethanol, and 1 mM EDTA. The crystals belonged to space group $P2_12_12_1$, with cell parameters $a = 44.2$ Å, $b = 50.1$ Å, $c = 123.3$ Å, and grew only rarely to suitable sizes; they were named "form-S."

At a later stage, we obtained a second crystal form with PEG. The drops were 7 mg/mL protein, 20 mM MOPS, pH 7.1, 9% (w/v) PEG-3350, 5 mM $MgSO_4$, 5 mM β-mercaptoethanol, 1 mM EDTA, and 0.02% NaN_3. The reservoir contained 20% (w/v) PEG-3350, 20 mM MOPS, pH 7.1, 5 mM β-mercaptoethanol, 1 mM EDTA, and 0.02% NaN_3. The crystals grew to sizes of $1{,}500 \times 400 \times 150$ μm^3. They belonged to the same space group with the same cell parameters (except for a 1.0-Å shorter *c*-axis) as form-S and were named "form-P." By dropping crystals into a calibrated gradient of bromobenzene and toluene, their density was determined to 1.17 $g \cdot cm^{-3}$. At an M_r of 25,500, this density corresponds to 1 molecule per crystallographic asymmetric unit and 54% solvent.

All X-ray diffraction data were collected with a multiwire area detector (Siemens, X1000) and Cu K_α radiation (Rigaku, RU200B). The native data set of crystal form-P was collected from five crystals at room temperature. The resolution limit was set by the 3σ criterion for 30% of the outermost reflections. This resulted in 261,709 measured reflections that were reduced to the 20,850 unique reflections stated in Table 1. Because crystal form-S was rare, we used only one large crystal for collecting all native data, comprising 81,251 reflections that were reduced to 15,064 uniques (Table 1).

For phasing, we produced four heavy atom derivatives (Table 4). The difference-Patterson of the MMA derivative could be interpreted and used for locating all other heavy atoms. The heavy atom parameters were refined, and the phases were improved by solvent flattening. The resulting electron density map was good enough to recognize α-helices that permitted placement of a polyalanine chain derived from the homologous yeast enzyme (Abele & Schulz, 1995). The structure was refined by simulated annealing using X-PLOR (Brünger et al., 1987). After four rounds, the main chain and all side chains of CORE and NMP_{bind}, as well as the chain fold of the LID domain, had been fitted. In 28 more rounds, all structural features were adjusted and solvent was added. For the structure of crystal form-S, we started with the final model of form-P, giving rise to an initial *R*-factor of 40%. The refinement ran through six rounds, resulting in smallish modifications of the polypeptide and changes of the water structure.

The coordinates and structure factors of AK2 are deposited in the Protein Data Bank, Brookhaven, New York under the accession codes 1AK2 and 2AK2.

Acknowledgments

We thank E. Schiltz and C. Vonrhein for discussions. The work was supported by the Deutsche Forschungsgemeinschaft under SFB-60.

References

Abele U, Schulz GE. 1995. High-resolution structures of adenylate kinase from yeast ligated with inhibitor Ap_5A, showing the pathway of phosphoryl transfer. *Protein Sci 4*:1262–1271.

Berry MB, Meador B, Bilderback T, Liang P, Glaser M, Phillips GN Jr. 1994. The closed conformation of a highly flexible protein: The structure of *E. coli* adenylate kinase with bound AMP and AMPPNP. *Proteins Struct Funct Genet 19*:183–198.

Brünger AT, Kuriyan J, Karplus M. 1987. Crystallographic *R*-factor refinement by molecular dynamics. *Science 235*:458–460.

Diederichs K, Schulz GE. 1991. The refined structure of the complex between adenylate kinase from beef heart mitochondrial matrix and its substrate AMP at 1.85 Å resolution. *J Mol Biol 217*:541–549.

Douglas MG, McCammon MT, Vassarotti A. 1986. Targeting proteins into mitochondria. *Microbiol Rev 50*:166–178.

Dreusicke D, Karplus PA, Schulz GE. 1988. Refined structure of porcine cytosolic adenylate kinase at 2.1 Å resolution. *J Mol Biol 199*:359–371.

Dreusicke D, Schulz GE. 1986. The glycine-rich loop of adenylate kinase forms a giant anion hole. *FEBS Lett 208*:301–304.

Font B, Gautheron DC. 1980. General and kinetic properties of pig heart mitochondrial adenylate kinase. *Biochim Biophys Acta 611*:299–308.

Frank R, Trosin M, Tomasselli AG, Noda L, Krauth-Siegel RL, Schirmer RH. 1986. Mitochondrial adenylate kinase (AK2) from bovine heart. The complete primary structure. *Eur J Biochem 154*:205–211.

Gerstein M, Schulz GE, Chothia C. 1993. Domain closure in adenylate ki-

nase. Joints on either side of two helices close like neighboring fingers. *J Mol Biol 229*:494–501.

Gilles AM, Glaser P, Perrier V, Meier A, Longin R, Sebald M, Maignan L, Pistotnik E, Bârzu O. 1994. Zinc, a structural component of adenylate kinases from gram-positive bacteria. *J Bacteriol 176*:520–523.

Glick B, Schatz G. 1991. Import of proteins into mitochondria. *Annu Rev Genet 25*:21–44.

Goelz SE, Cronan JE Jr. 1982. Adenylate kinase of *Escherichia coli*: Evidence for a functional interaction in phospholipid synthesis. *Biochemistry 21*:189–195.

Greschik H. 1994. Protein-Engineering zur Verbesserung von Kristallkontakten in Kristallen der Adenylatkinase Isoenzyme 2 [diploma thesis]. Freiburg im Breisgau, Germany: Albert-Ludwigs-Universität.

Heil A, Müller G, Noda LH, Pinder T, Schirmer RH, von Zabern I. 1974. The amino acid sequence of porcine adenylate kinase from skeletal muscle. *Eur J Biochem 43*:131–144.

Jäger I. 1985. Isolierung, Reinigung und Trennung der Isoenzyme der Adenylatkinase aus Rinderlebermitochondrien und Vergleich mit dem Enzym aus Rinderherz [diploma thesis]. Freiburg im Breisgau, Germany: Albert-Ludwigs-Universität.

Kishi F, Tanizawa Y, Nakazawa A. 1987. Isolation and characterization of two types of cDNA for mitochondrial adenylate kinase and their expression in *Escherichia coli*. *J Biol Chem 262*:11785–11789.

Kuby SA, Palmieri RH, Frischat AH, Wu LH, Maland L, Manship M. 1984. Studies on adenosine triphosphate transphosphorylase. Amino acid sequence of rabbit muscle ATP:AMP transphosphorylase. *Biochemistry 23*:2392–2399.

Laskowski RA, MacArthur MW, Moss DS, Thornton JM. 1993. PROCHECK: A program to check the stereochemical quality of protein structures. *J Appl Crystallogr 26*:283–291.

Luzzati V. 1952. Traitement statistique des erreurs dans la determination des structures cristallines. *Acta Crystallogr 5*:802–810.

Magdolen V, Schricker R, Strobel G, Germaier H, Bandlow W. 1992. In vivo import of yeast adenylate kinase into mitochondria affected by site-directed mutagenesis. *FEBS Lett 299*:267–272.

Markland FS, Wadkins CL. 1966. Adenosine triphosphate-adenosine 5′-monophosphate phosphotransferase of bovine liver mitochondria. Isolation and chemical properties. *J Biol Chem 241*:4124–4135.

Miyoshi K, Egi Y, Shioda T, Kawasaki T. 1990. Evidence for in vitro synthesis of thiamin triphosphate by cytosolic adenylate kinase in chicken skeletal muscle. *J Biochem 108*:267–270.

Müller CW, Schulz GE. 1992. Structure of the complex between adenylate kinase from *E. coli* and the inhibitor Ap_5A refined at 1.9 Å resolution. *J Mol Biol 224*:159–177.

Müller-Dieckmann HJ, Schulz GE. 1995. Substrate specificity and assembly of the catalytic center derived from the two structures of ligated uridylate kinase. *J Mol Biol 246*:522–530.

Nicholls A, Sharp KA, Honig B. 1991. Protein folding and association: Insights from the interfacial and thermodynamical properties of hydrocarbons. *Proteins Struct Funct Genet 11*:281–296.

Noda LH. 1973. Adenylate kinase. In: Boyer PD, ed. *The enzymes, vol 8A*. New York: Academic Press. pp 279–305.

Read RJ. 1986. Improved Fourier coefficients for maps using phases from partial structures with errors. *Acta Crystallogr A 42*:140–149.

Schneemann A. 1986. Reinigung, Charakterisierung und Kristallisation der großen und kleinen Variante der Adenylatkinase aus dem Intermembranraum von Rinderlebermitochondrien [diploma thesis]. Freiburg im Breisgau, Germany: Albert-Ludwigs-Universität.

Schulz GE, Mueller CW, Diederichs K. 1990. Induced-fit movements in adenylate kinases. *J Mol Biol 213*:627–630.

Spuergin P, Abele U, Schulz GE. 1995. Stability, activity and structure of adenylate kinase mutants. *Eur J Biochem 231*:405–413.

Stehle T, Schulz GE. 1992. Refined structure of the complex between guanylate kinase and its substrate GMP at 2.0 Å resolution. *J Mol Biol 224*:1127–1141.

Tanabe T, Yamada M, Noma T, Kajii T, Nakazawa A. 1993. Tissue-specific and developmentally regulated expression of the genes encoding adenylate kinase isozymes. *J Biochem 113*:200–207.

Tanaka H, Yamada M, Kishi F, Nakazawa A. 1990. Isolation and characterization of the gene encoding bovine adenylate kinase isoenzyme 2. *Gene 93*:221–227.

Tomasselli AG, Frank R, Schirmer RH. 1986. The complete primary structure of GTP:AMP phosphotransferase from beef-heart mitochondria. *FEBS Lett 202*:303–308.

Tomasselli AG, Noda LH. 1980. Mitochondrial ATP:AMP phosphotransferase from beef heart; purification and properties. *Eur J Biochem 103*:481–491.

Vonrhein C, Schlauderer GJ, Schulz GE. 1995. Movie of the structural changes during a catalytic cycle of nucleoside monophosphate kinases. *Structure 3*:483–490.

Watenpaugh KD, Sieker LC, Jensen LH. 1980. Crystallographic refinement of rubredoxin at 1.2 Å resolution. *J Mol Biol 138*:615–633.

Wild K, Bohner T, Aubry A, Folkers G, Schulz GE. 1995. The three-dimensional structure of thymidine kinase from Herpes simplex virus type 1. *FEBS Lett 368*:289–292.

Yamada M, Shahjahan M, Tanabe T, Kishi F, Nakazawa A. 1989. Cloning and characterization of cDNA for mitochondrial GTP:AMP phosphotransferase of bovine liver. *J Biol Chem 264*:19192–19199.